THE DYNAMICS AND CONTROL OF

LARGE FLEXIBLE SPACE STRUCTURES

Peter M. Bainum, V. K. Kumar, R. Krishna,
A. S. S. R. Reddy, and C. M. Diarra
Howard University
Washington, D. C.

INTRODUCTION

Large, flexible orbiting systems have been proposed for possible use in communications, electronic orbital-based mail systems, and solar energy collection. The size and low weight-to-area ratio of such systems indicate that system flexibility is now the main consideration in the dynamics and control problem. For such large, flexible systems, both orientation and surface shape control will often be required.

Figure 1 illustrates a conceptual development plan of a system software capability for use in the analysis of the dynamics and control of large space structures technology (LSST) systems. This concept can be subdivided into four different stages: (1) system dynamics; (2) structural dynamics; (3) application of control algorithms; and (4) simulation of environmental disturbances. Modeling the system dynamics of such systems in orbit is the most fundamental component.

SOLAR RADIATION PRESSURE EFFECTS

The equations for determining the effects of solar radiation pressure on a flexible beam are summarized below.

Forces:

$$\bar{F}_a = -h_o \bar{\tau} \int_s (\hat{\tau} \cdot \hat{n})\, ds \qquad \text{(absorbing surface)}$$

$$\bar{F}_\gamma = -2h_o \int_s \hat{n}(\hat{\tau} \cdot \hat{n})^2\, ds \qquad \text{(reflecting surface)}$$

$$\bar{F}_\varepsilon = \bar{F}_a + \varepsilon(\bar{F}_\gamma - \bar{F}_a) \qquad \text{(surface with reflectivity } \varepsilon\text{)}$$

Moments:

$$\bar{M}_a = h_o \hat{\tau} x \int_s \bar{R}(\hat{\tau} \cdot \hat{n})\, ds \qquad \text{(absorbing surface)}$$

$$\bar{M}_\gamma = 2h_o \int_s \hat{n} \times \bar{R}(\hat{\tau} \cdot \hat{n})^2\, ds \qquad \text{(reflecting surface)}$$

$$\bar{M}_\varepsilon = \bar{M}_a + \varepsilon(\bar{M}_\gamma - \bar{M}_a) \qquad \text{(surface with reflectivity } \varepsilon\text{)}$$

where

$\hat{\tau}$ = unit vector in the direction of solar radiation

$\hat{n}$ = unit vector normal to the surface ds

$h_o = 4.64 \times 10^{-6}$ N/m^2

Results for a flexible beam:

$$\bar{F}_a = -a_o h_o \left[a_o(z_1 - z_o) - b_o\right]\hat{i} + h_o b_o \left[a_o(z_1 - z_o) - b_o\right]\hat{k}$$

$$\bar{M}_a = -h_o a_o b_o \left\{(z_1 + z_o)/2 - 2/\Omega_n \left[\sigma(\cos h\Omega_n - \cos \Omega_n)\right] + \sin \Omega_n + \sin h\Omega_n\right\}$$

$$\bar{F}_\gamma = -2h_o \int_s z' \frac{(a_o z' - b_o)^2}{(1 + z')^2} dx\, \hat{i} - 2h_o \int_s \frac{(a_o z' - b_o)^2}{(1 + z')^2} dx\, \hat{k}$$

$$\bar{M}_\gamma = 2h_o \int_s \frac{(a_o z' - b_o)^2}{(1 + z')^2} \left(z'z - x + \frac{1}{2}\right) dx\, \hat{k}$$

where

$a_o = \sin \theta \qquad b_o = \cos \theta$

$z(x)$ = flexural deflection

$z' = \frac{dz}{dx}$

Ω_n = nth modal frequency

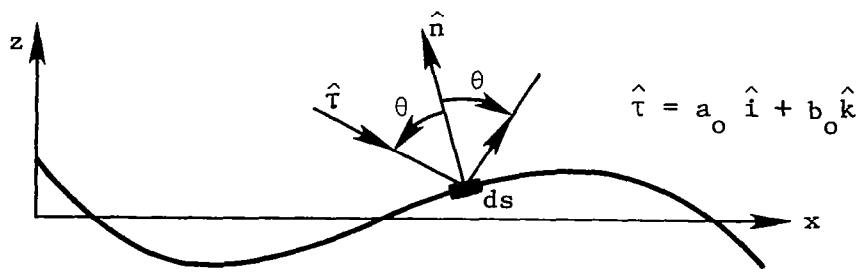

Figure 2 shows the variation of the resultant horizontal and normal force components of a beam with a completely absorbing surface as the solar incidence angle θ is varied from 0^o to 90^o. Here, θ represents the angle between the normal to the undeflected beam and $\bar{\tau}$. The horizontal and normal force components are measured relative to the beam's undeflected axes. As expected, for small tip deflections of the beam, the resultant horizontal absorbing force component becomes zero for incidence angles of 0^o and 90^o, while the normal component has a maximum amplitude at zero incidence angle. In figures 2 and 3 the individual effect of each mode is illustrated, with the assumed beam tip deflection as indicated in the figures.

The magnitude of the resultant moments as the solar incidence angle is varied is shown in figure 3 for the assumed tip deflection of 0.01ℓ. Large moments can result for larger deflections, whereas these moments would be zero for a rigid beam. For small pitch angle displacements, the moment due to solar radiation pressure may become greater than the moment due to the gravity-gradient forces, as shown in figure 4. It is seen that at geosynchronous altitudes, the moment due to solar radiation may become predominant even for deflections on the order of 0.01ℓ. With the aid of moment diagrams such as those in figure 3, it is possible to determine the disturbance torques due to solar radiation pressure once the number of modes and the associated modal deflections are specified for a model.

MODELING ERRORS - ORBITAL AND GRAVITY-GRADIENT EFFECTS

One of the principal sources of (disturbance) torques acting on an orbiting space structure is the orbital (gyroscopic) and gravity-gradient effects. Such effects associated with the orbital (angular) motion do not need to be considered when developing a system model for an Earth-based large flexible system. Many investigators, however, model the pitch, roll, and yaw modes (rigid body motion) of large, flexible orbiting systems as double integrator plants (two poles at the origin), and the subsequent control system design is based on these models. It is the purpose of this section to evaluate the effects of omitting the orbital and gravity-gradient effects when designing shape and orientation control laws for flexible systems in orbit. Models of flexible square plates and shallow spherical shells in orbit are selected as examples.

The effects of designing control laws without the orbital and gravity-gradient torques included in the system models of square plates and shallow spherical shells in low Earth orbit (250 nautical miles) are illustrated in figures 5 to 10. A square plate was also considered in a geosynchronous orbit. The analysis was performed by first calculating the control law, which was in the form $\bar{u} = F\bar{x}$, for the case where the orbital and gravity-gradient effects are not included in the model. The same control law is then applied to the model that includes these effects.

For figure 4, the control law was selected such that the overall response time constant of the system is 2.22 hours (which may be reasonable for a large space structure). The shift in the closed loop poles of the plate model due to the presence of the orbital and gravity-gradient effects is illustrated in this figure. It can be seen that some of the poles move to the right half plane, leading to instability and thus emphasizing the importance of including the orbital and gravity-gradient effects in the model. The poles due to the rigid body modes are shifted considerably, but the flexible modes remain virtually unaffected. This can be attributed to the high frequency of the flexible modes. (Note that the orbital and gravity-gradient effects are of a relatively low frequency.) This result gives an

indication that by designing a more robust (faster response) control system, the shift of the actual closed loop poles would be relatively less pronounced.

This phenomenon can be demonstrated by designing the gain matrix, F, such that the desired response time constant is reduced to 460 seconds. The shift in the closed loop poles for this case is shown in figure 6. In figure 7 the control forces are shown for the second (more robust) control law, where the closed loop response with orbital and gravity-gradient effects is degraded but does not become unstable. (It should be noted that time has been nondimensionalized with respect to the orbital frequency of the 250-nautical-mile low Earth orbit, in order to provide a basis for comparison.) The difference in the total control force impulse as applied to the two models (a) and (b) is minimal because of the robustness of the controller. The slowly varying orbital and gravity-gradient torques have a relatively greater impact on the less robust systems, and can even lead to possible instabilities, as was illustrated in figure 5.

As expected, the orbital and gravity-gradient effects are less pronounced in the case of a structure in geosynchronous orbit than in the case of a structure in low Earth orbit. However, if the control systems are designed with response times comparable to the orbital periods, under the influence of orbital and gravity-gradient effects the closed loop systems may become unstable.

The shift in the closed loop poles of the spherical shell model due to the presence of the orbital and gravity-gradient effects is shown in figure 8. One of the closed loop poles is moved to the right-hand side of the S-plane, causing instability. As compared to the case of the plate, the effect of the orbital and gravity-gradient torques on the shell is more pronounced, as the instability due to movement of the poles occurs at the relatively fast designed response time constant of 615 seconds (compared to 8000 seconds in the case of plate). When the control is redesigned for a response time constant of 400 seconds, the shift in the poles is as shown in figure 9. A general shift in the rigid body motion poles is observed, but the system remains stable.

The control forces associated with both models (a) and (b) of figure 9 are compared in figure 10. A considerable increase in the control effort is observed when the model includes the effect of the orbital gyroscope and gravity-gradient torques. This may be explained by the fact that the mass distribution of the shell is more complex than that of the plate, resulting in relatively greater dynamic coupling when the gyroscopic and gravity-gradient effects are included in the shell model.

THE DEVELOPMENT OF AN ALGORITHM TO EVALUATE COUPLING COEFFICIENTS FOR A LARGE FLEXIBLE ANTENNA

The generic mode equations and the equations of rotational motion of a flexible orbiting body contain both coupling terms between the rigid and flexible modes and terms due to the coupling within the flexible modes that are assumed to be small and thus are usually neglected when a finite element analysis of the dynamics of the system is undertaken. In this section a computational algorithm is developed which permits the evaluation of the coefficients in these coupling terms in the equations of motion as applied to a finite element model of a hoop/column antenna system (ref. 1).

Using a Newton-Euler approach, one can express the equations of motion of an elemental mass of the system, in the frame moving with the body, as:

$$\left\{\bar{a}_{cm} + \ddot{\bar{r}} + 2\bar{\omega} + \dot{\bar{r}} + \dot{\bar{\omega}} \times \bar{r} + \bar{\omega} \times (\bar{\omega} \times \bar{r})\right\}\rho \, dv = \left\{\bar{f} + \bar{e} + L(\bar{q})/\rho\right\}\rho \, dv \qquad (1)$$

where

ρ = mass per unit volume

$\bar{e}$ = external forces per unit mass

$\bar{q}$ = elastic transverse displacements of the element of volume

$\bar{f}$ = force due to the gravity on the unit mass

L = the linear operator which when applied to $\bar{q}$ yields the elastic forces acting on the element of volume considered

$\bar{r}$ = position vector of element dv

$\bar{\omega}$ = inertial angular velocity of the body frame

$\bar{a}_{cm}$ = acceleration of the center of mass

Equations of Rotational Motion

The equations of rotational motion of the body are obtained by taking the moments of all the external, internal, and inertial forces acting on the body; i.e., from equation (1):

$$\int \bar{r} \times \left[\bar{a}_{cm} + \ddot{\bar{r}} + (2\bar{\omega} \times \dot{\bar{r}}) + (\dot{\bar{\omega}} \times \bar{r}) + \left(\bar{\omega} \times (\bar{\omega} \times \bar{r})\right)\right] \rho \, dv = \int_v \bar{r} \times \left[L(\bar{q})/\rho + \bar{f} + \bar{e}\right]\rho \, dv \qquad (2)$$

One can obtain the following form for the equations of rotational motion:

$$\bar{R} + \sum_{n=1}^{\infty} \bar{Q}^{(n)} + \sum_{n=1}^{\infty} \bar{D}^{(n)} = \bar{G}_R + \sum_{n=1}^{\infty} \bar{G}^{(n)} + \bar{C} \qquad (3)$$

where

$$\bar{R} = \int_v \left[\bar{r}_o \times (\dot{\bar{\omega}} \times \bar{r}_o) - (\bar{r}_o \cdot \bar{\omega})(\bar{\omega} \times \bar{r}_o)\right] \rho \, dv$$

$$\sum_{n=1}^{\infty} \bar{Q}^{(n)} = \int_v \left\{ \bar{r}_o \times \ddot{\bar{q}} + 2\bar{r}_o \times \left(\bar{\omega} \times \dot{\bar{q}}\right) + \bar{r}_o \times \left(\dot{\bar{\omega}} \times \bar{q}\right) + \bar{q} \times \left(\dot{\bar{\omega}} \times \bar{r}_o\right) \right.$$
$$\left. - \left(\bar{r}_o \cdot \bar{\omega}\right)\left[\left(\bar{\omega} \times \bar{q}\right) - \left(\bar{q} \cdot \bar{\omega}\right)\right]\left(\bar{\omega} \times \bar{r}_o\right) \right\} \rho \, dv$$

$$\sum_{n=1}^{\infty} \bar{D}^{(n)} = \int_v \bar{q}\rho \, dv \times \left(\bar{a}_{cm} - \bar{f}_o\right) + \sum_{n=1}^{\infty} \omega_n^2 A_n \int_v \bar{r}_o \times \bar{\Phi}^{(n)} \rho \, dv$$

$$\bar{G}_R = \int \bar{r}_o \times M\bar{r}_o \, \rho \, dv$$

$$\sum_{n=1}^{\infty} \bar{G}^{(n)} = \int_v \left(\bar{r}_o \times M\bar{q} + \bar{q} \times M\bar{r}_o\right)\rho \, dv$$

$$\bar{C} = \int_v \bar{r} \times \bar{e} \, \rho \, dv$$

$$\bar{r} = \bar{r}_o + \bar{q}$$

M = matrix operator which when applied to $\bar{r}$ yields gravity-gradient forces

$\bar{a}_{cm}$ = acceleration of the center of mass

$\bar{f}_o$ = force/mass due to gravity at the undeformed center of mass

$\bar{\Phi}^{(n)}$ = modal shape vector for the nth mode

ω_n = frequency of the nth mode

A_n = time-dependent modal amplitude function

Generic Mode Equations

The generic mode equation is obtained by taking the modal components of all internal, external, and inertial forces acting on the body, i.e.,

$$\int_v \bar{\Phi}^{(n)} \cdot \left[\bar{a}_{cm} + \ddot{\bar{r}} + 2\bar{\omega} \times \dot{\bar{r}} + \dot{\bar{\omega}} \times \bar{r} + \bar{\omega} \times \left(\bar{\omega} \times \bar{r}\right)\right] \rho \, dv$$
$$= \int_v \bar{\Phi}^{(n)} \cdot \left[L(\bar{q})/\rho + \bar{f} + \bar{e}\right]\rho \, dv \qquad (4)$$

The generic mode equation is obtained in the following form:

$$\ddot{A}_n + \omega_n^2 A_n + \psi_n/M_n + \sum_{m=1}^{\infty} \psi_{mn}/M_n = \left(g_n + \sum_{m=1}^{\infty} g_{mn} + E_n + D_n'\right)\Big/ M_n \qquad (5)$$

where

$$\psi_n = \int_v \left[\bar{\Phi}^{(n)} \cdot \dot{\bar{\omega}} \times \bar{r}_o + \bar{\Phi}^{(n)} \cdot \bar{\omega} \times (\bar{\omega} \times \bar{r}_o)\right] \rho \, dv$$

$$\sum_{m=1}^{\infty} \psi_{mn} = \int_v \left[2\bar{\Phi}^{(n)} \cdot \bar{\omega} \times \dot{\bar{q}} + \bar{\Phi}^{(n)} \cdot \dot{\bar{\omega}} \times \bar{q} + \bar{\Phi}^{(n)} \cdot \bar{\omega} \times (\bar{\omega} \times \bar{q})\right] \rho \, dv$$

$$g_n = \int \bar{\Phi}^{(n)} \cdot M\bar{r}_o \, \rho \, dv$$

$$\sum_{m=1}^{\infty} g_{mn} = \int_v \bar{\Phi}^{(n)} \cdot M\bar{q}\rho \, dv$$

$$E_n = \int \bar{\Phi}^{(n)} \cdot \bar{e}\rho \, dv$$

$$D_n' = \int_v \bar{\Phi}^{(n)} \rho \, dv \cdot (\bar{a}_{cm} - \bar{f}_o)$$

Here ψ_n is the inertia coupling between rigid body modes and the nth structural mode and ψ_{mn} is the inertia coupling between the mth and nth structural modes.

Cartesian Components of the Different Coupling Terms

The expressions for $\bar{R}$, $\bar{Q}^{(n)}$, $\bar{G}_R$, $\bar{G}^{(n)}$, ψ_n, ψ_{mn}, g_n, and g_{mn} in Cartesian components are presented in this section. The following vectors can be expressed in their Cartesian component form as:

$$\bar{r}_o = \xi_x \hat{i} + \xi_y \hat{j} + \xi_z \hat{k}; \quad \bar{\omega} = \omega_x \hat{i} + \omega_y \hat{j} + \omega_z \hat{k}$$

$$\bar{q} = \sum_{n=1}^{\infty} A_n(t)\bar{\Phi}^{(n)}(\bar{r}_o); \quad \bar{\Phi}^{(n)} = \phi_x^{(n)}\hat{i} + \phi_y^{(n)}\hat{j} + \phi_z^{(n)}\hat{k}$$

$$\bar{Q}^{(n)} = Q_x^{(n)}\hat{i} + Q_y^{(n)}\hat{j} + Q_z^{(n)}\hat{k}$$

$$\bar{G}^{(n)} = G_x^{(n)}\hat{i} + G_y^{(n)}\hat{j} + G_z^{(n)}\hat{k}$$

where $\hat{i}$, $\hat{j}$, and $\hat{k}$ are unit vectors along the body principal axes of inertia in the undeformed state, and ξ_x, ξ_y, and ξ_z are the coordinates of a point in the undeformed state.

With the use of the component forms of the vectors given above, one can expand the various vector expressions given in equations (3) and (5) to obtain

$$\bar{R} = \left[J_x\dot{\omega}_x + (J_z - J_y)\omega_y\omega_z\right]\hat{i} + \left[J_y\dot{\omega}_y + (J_x - J_z)\omega_z\omega_x\right]\hat{j} + \left[J_z\dot{\omega}_z + (J_y - J_x)\omega_x\omega_y\right]\hat{k} \tag{6}$$

$$\begin{aligned} Q_x^{(n)} = {} & \ddot{A}_n\left(H_{yz}^{(n)} - H_{zy}^{(n)}\right) + 2\dot{A}_n\left[\left(H_{yy}^{(n)} + H_{zz}^{(n)}\right)\omega_x - H_{yx}^{(n)}\omega_y - H_{zx}^{(n)}\omega_z\right] \\ & + A_n\left[2\left(H_{yy}^{(n)} + H_{zz}^{(n)}\right)\dot{\omega}_x - \left(H_{xy}^{(n)} + H_{yx}^{(n)}\right)\dot{\omega}_y - \left(H_{zx}^{(n)} + H_{xz}^{(n)}\right)\dot{\omega}_z\right. \\ & - 2\omega_y\omega_z\left(H_{zz}^{(n)} - H_{yy}^{(n)}\right) - \omega_x\omega_y\left(H_{xz}^{(n)} + H_{zx}^{(n)}\right) + \omega_x\omega_z\left(H_{xy}^{(n)} + H_{yx}^{(n)}\right) \\ & \left. + \left(\omega_z^2 - \omega_y^2\right)\left(H_{yz}^{(n)} + H_{zy}^{(n)}\right)\right] \end{aligned} \tag{7}$$

$$\bar{G}_R = (J_z - J_y)M_{23}\hat{i} + (J_x - J_z)M_{31}\hat{j} + (J_y - J_x)M_{21}\hat{k} \tag{8}$$

$$G_x^{(n)} = A_n\Big[(M_{33} - M_{22})\Big(H_{yz}^{(n)} + H_{zy}^{(n)}\Big) - M_{21}\Big(H_{xz}^{(n)} + H_{zx}^{(n)}\Big)$$

$$+ M_{31}\Big(H_{xy}^{(n)} + H_{yx}^{(n)}\Big) + 2M_{23}\Big(H_{yy}^{(n)} - H_{zz}^{(n)}\Big)\Big] \tag{9}$$

$$\psi_n = \dot{\omega}_x\Big(H_{yz}^{(n)} + H_{zy}^{(n)}\Big) + \dot{\omega}_y\Big(H_{zx}^{(n)} - H_{xz}^{(n)}\Big) + \dot{\omega}_z\Big(H_{xy}^{(n)} - H_{yx}^{(n)}\Big)$$

$$+ \omega_x\omega_y\Big(H_{xy}^{(n)} + H_{yx}^{(n)}\Big) + \omega_y\omega_z\Big(H_{yz}^{(n)} + H_{zy}^{(n)}\Big) + \omega_z\omega_x\Big(H_{zx}^{(n)} + H_{xz}^{(n)}\Big)$$

$$- \omega_x^2\Big(H_{yy}^{(n)} + H_{zz}^{(n)}\Big) - \omega_y^2\Big(H_{zz}^{(n)} + H_{xx}^{(n)}\Big) - \omega_z^2\Big(H_{xx}^{(n)} + H_{yy}^{(n)}\Big) \tag{10}$$

$$\psi_{mn} = 2\dot{A}_m\Big[\omega_x\Big(L_{yz}^{(mn)} - L_{zy}^{(mn)}\Big) + \omega_y\Big(L_{zx}^{(mn)} - L_{xz}^{(mn)}\Big) + \omega_z\Big(L_{xy}^{(mn)} - L_{yx}^{(mn)}\Big)\Big]$$

$$+ A_m\Big[\dot{\omega}_x\Big(L_{yz}^{(mn)} - L_{zy}^{(mn)}\Big) + \dot{\omega}_y\Big(L_{zx}^{(mn)} - L_{xz}^{(mn)}\Big) + \dot{\omega}_z\Big(L_{xy}^{(mn)} - L_{yx}^{(mn)}\Big)$$

$$+ \omega_x\omega_y\Big(L_{xy}^{(mn)} + L_{yx}^{(mn)}\Big) + \omega_y\omega_z\Big(L_{yz}^{(mn)} + L_{zy}^{(mn)}\Big) + \omega_z\omega_x\Big(L_{zx}^{(mn)} + L_{xz}^{(mn)}\Big)$$

$$- \omega_x^2\Big(L_{yy}^{(mn)} + L_{zz}^{(mn)}\Big) - \omega_y^2\Big(L_{zz}^{(mn)} + L_{xx}^{(mn)}\Big) - \omega_z^2\Big(L_{xx}^{(mn)} + L_{yy}^{(mn)}\Big)\Big] \tag{11}$$

$$g_n = \sum_{\alpha\beta}\sum H_{\alpha\beta}^{(n)} M_{\alpha\beta}$$

$$g_{mn} = A_m \sum_{\alpha\beta}\sum L_{\alpha\beta}^{(mn)} M_{\alpha\beta}$$

where

$$H_{\alpha\beta}^{(n)} = \int_v \xi_\alpha \phi_\beta^{(n)} dm$$

$$L_{\alpha\beta}^{(mn)} = \int_v \phi_\alpha^{(m)} \phi_\beta^{(n)} dm$$

$\alpha, \beta = x, y, z$ or $1, 2, 3$

When α is x in $H_{\alpha\beta}^{(n)}$ or $L_{\alpha\beta}^{(mn)}$, the corresponding value of α in $M_{\alpha\beta}$ is 1. In a similar manner, when α is y in $H_{\alpha\beta}^{(n)}$ or $L_{\alpha\beta}^{(mn)}$, α is 2 in $M_{\alpha\beta}$, and when α is z in $H_{\alpha\beta}^{(n)}$ or $L_{\alpha\beta}^{(mn)}$, α is 3 in $M_{\alpha\beta}$. The same reasoning holds for β.

The expressions for $Q_y^{(n)}$ and $Q_z^{(n)}$ are obtained by the cyclic permutation of x, y, z in the expression for $Q_x^{(n)}$ in equation (7), and the expressions for $G_y^{(n)}$ and $G_z^{(n)}$ are obtained by the cyclic permutation of x, y, z in the expression for $G_x^{(n)}$ in equation (9).

For a discretized model, the expressions for the volume integrals are replaced by the following summations:

$$H_{\alpha\beta}^{(n)} = \sum_{i=1}^{k} (\xi_\alpha)_i \left(\phi_\beta^{(n)}\right)_i m_i \qquad (12)$$

$$(\alpha,\beta = x,y,z)$$

$$L_{\alpha\beta}^{(mn)} = \sum_{i=1}^{k} \left(\phi_\alpha^{(m)}\right)_i \left(\phi_\beta^{(n)}\right)_i m_i \qquad (13)$$

where

k = total number of discrete masses

i = index identifying a nodal point

m_i = mass concentrated at the ith node

ξ_α = coordinates of m_i in the undeformed state

REFERENCE

1. Bainum, Peter M.; Reddy, A. S. S. R.; Krishna, R.; Diarra, Cheick M.; and Kumar, V. K.: The Dynamics and Control of Large Flexible Space Structures - V. NASA CR-169360, 1982.

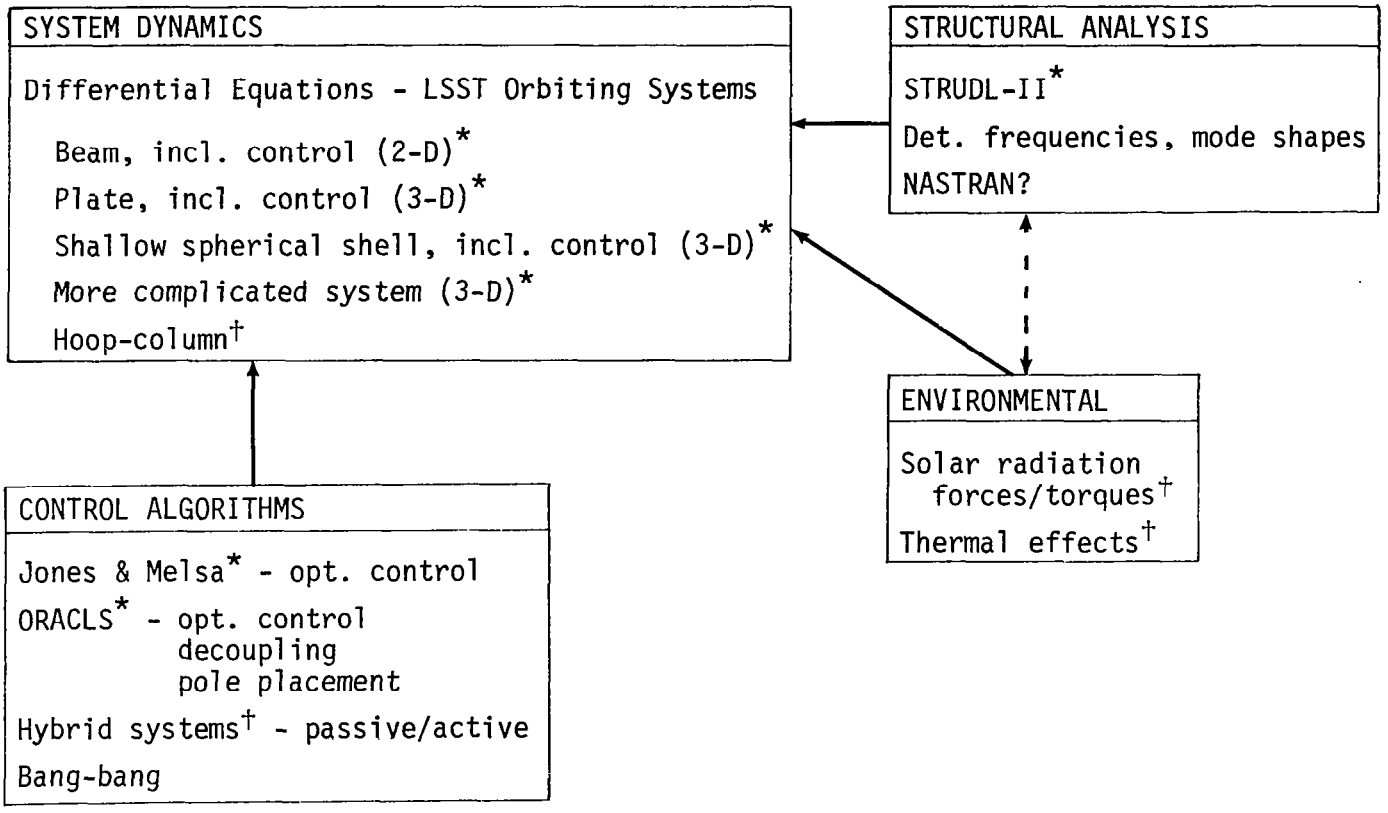

*Operational.
†In progress.

Figure 1.- Development of system software for LSST dynamics analysis.

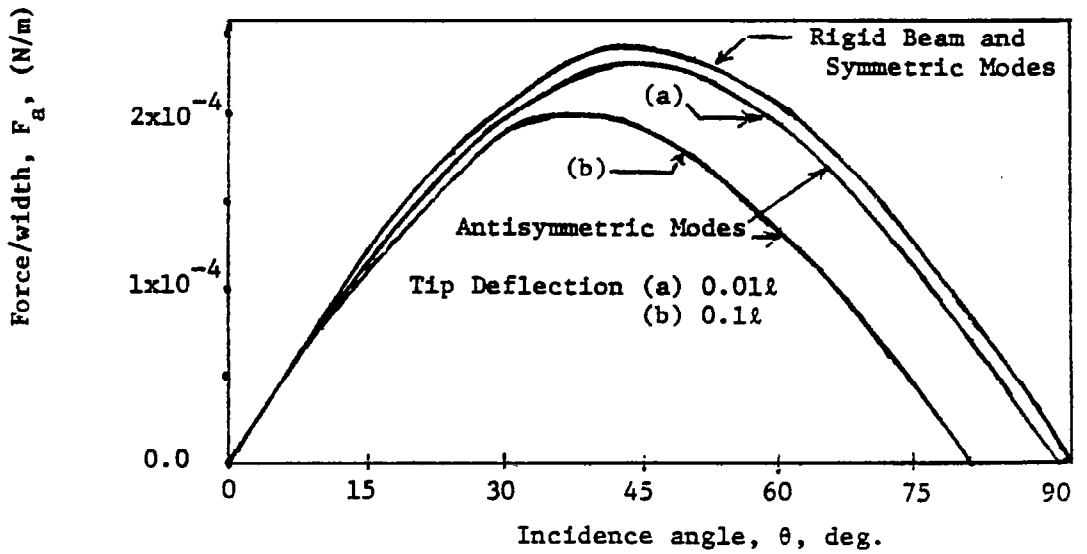

(a) Horizontal component.

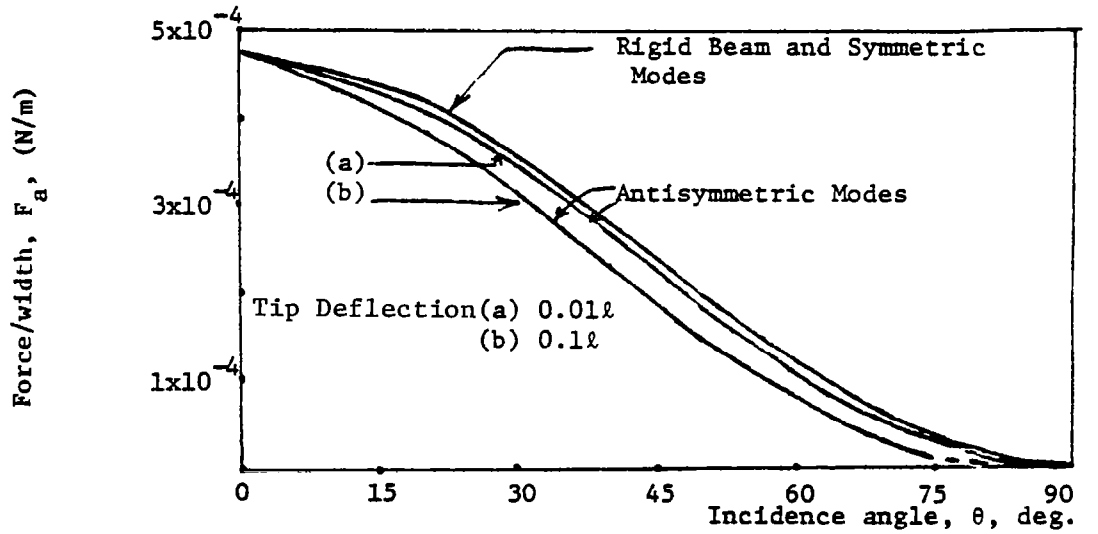

(b) Normal component.

Figure 2.- Variation of solar force components with incidence angle. Totally absorbing surface - free-free beam (length ℓ = 100 m).

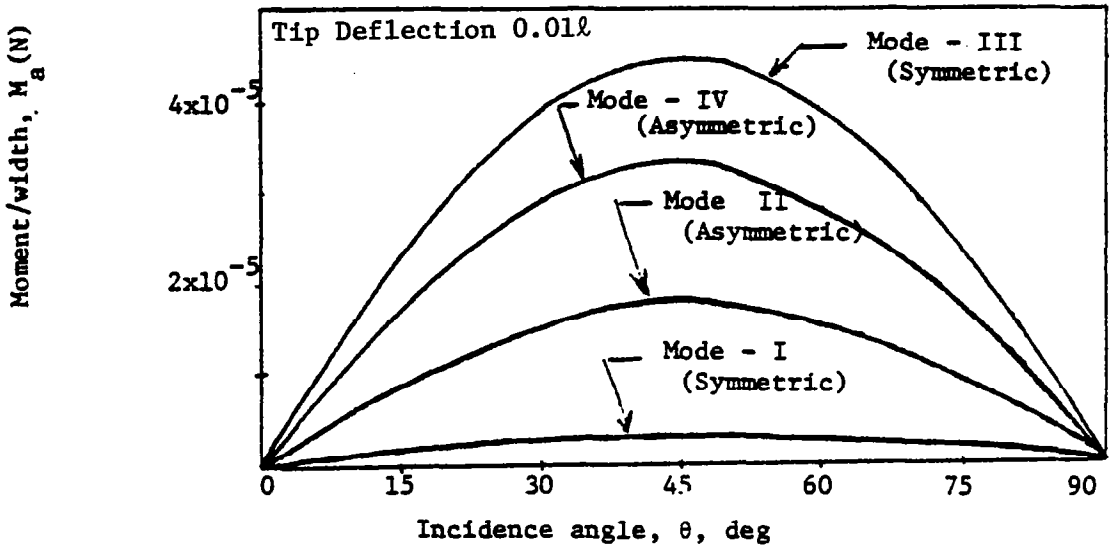

Figure 3.- Pitch moment due to solar radiation pressure (completely absorbing surface). Effect of individual modes in the system - free-free beam.

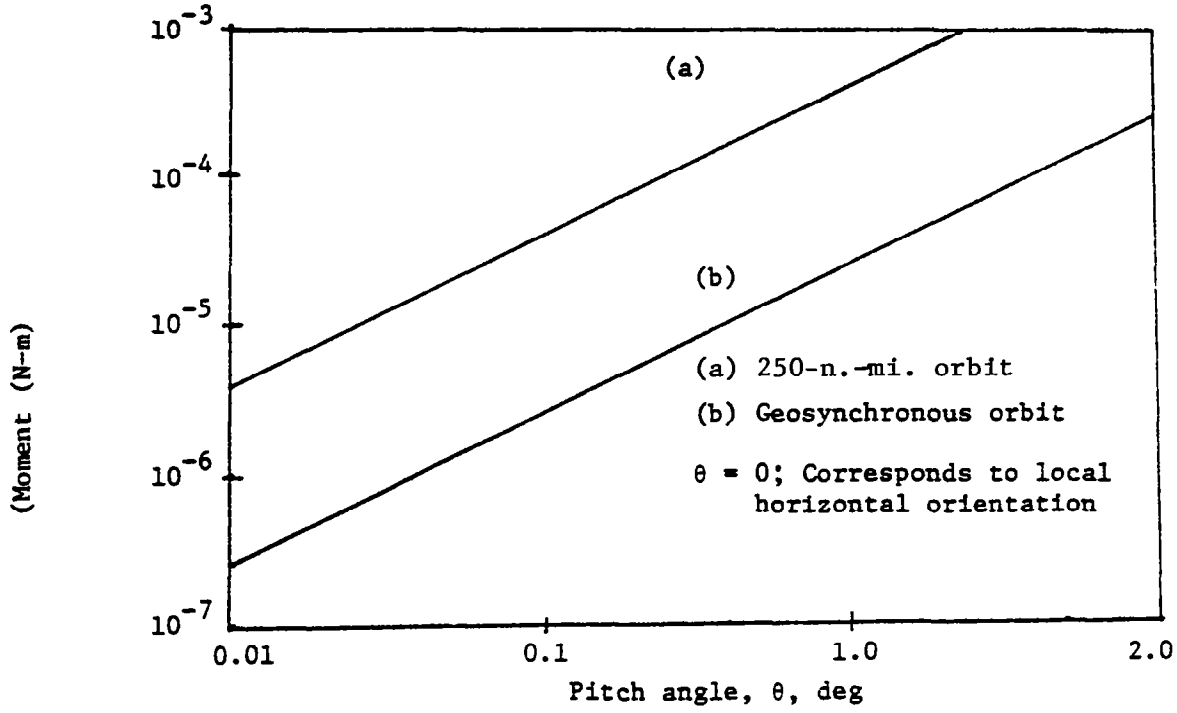

Figure 4.- Moment due to gravity-gradient force as a function of pitch angle (100-m rigid beam).

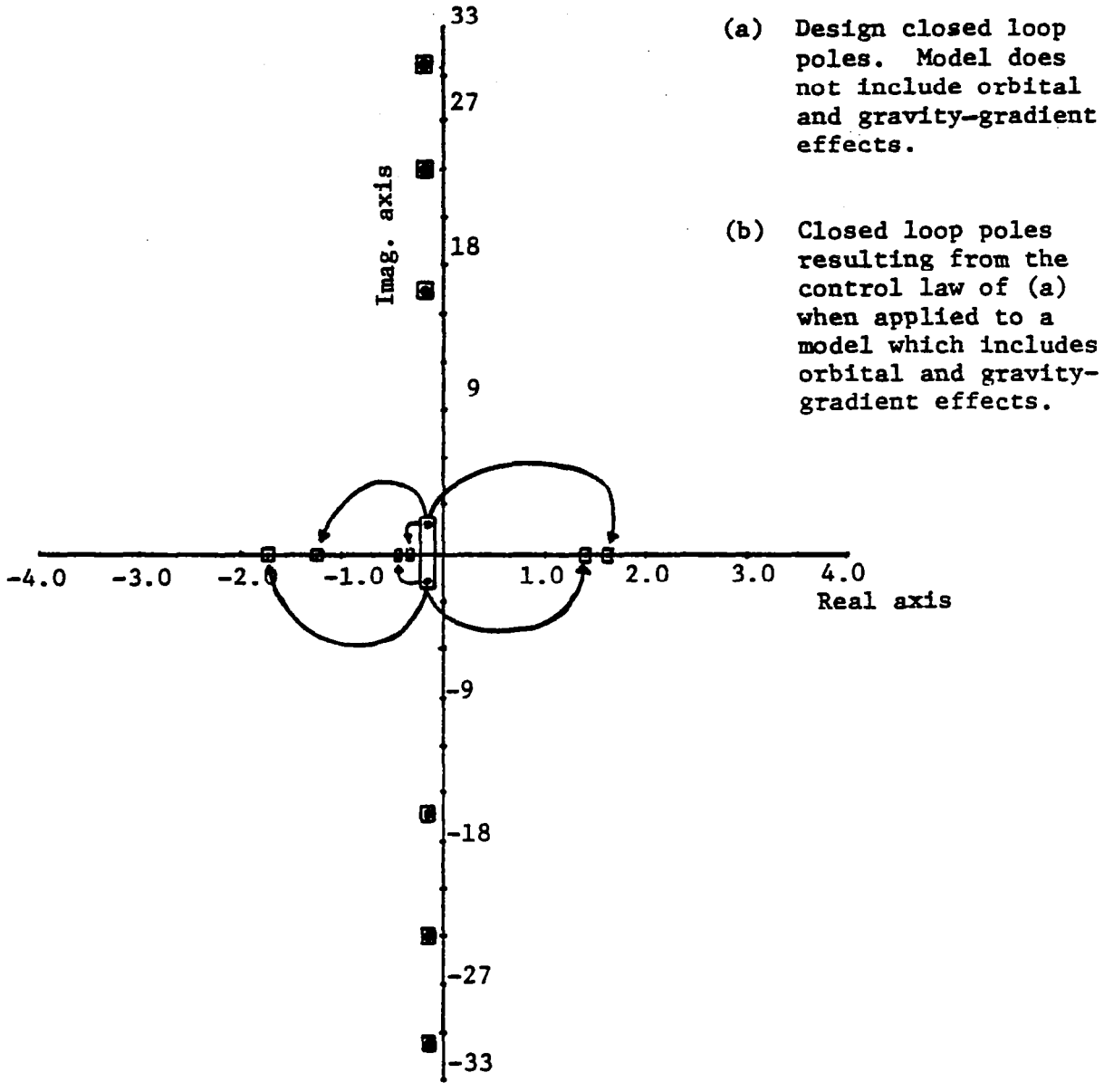

Figure 5.- Shift in closed loop poles due to orbital and gravity-gradient torques. Square plate in 250-n.-mi. orbit. Overall designed response time constant of the system = 8000 sec.

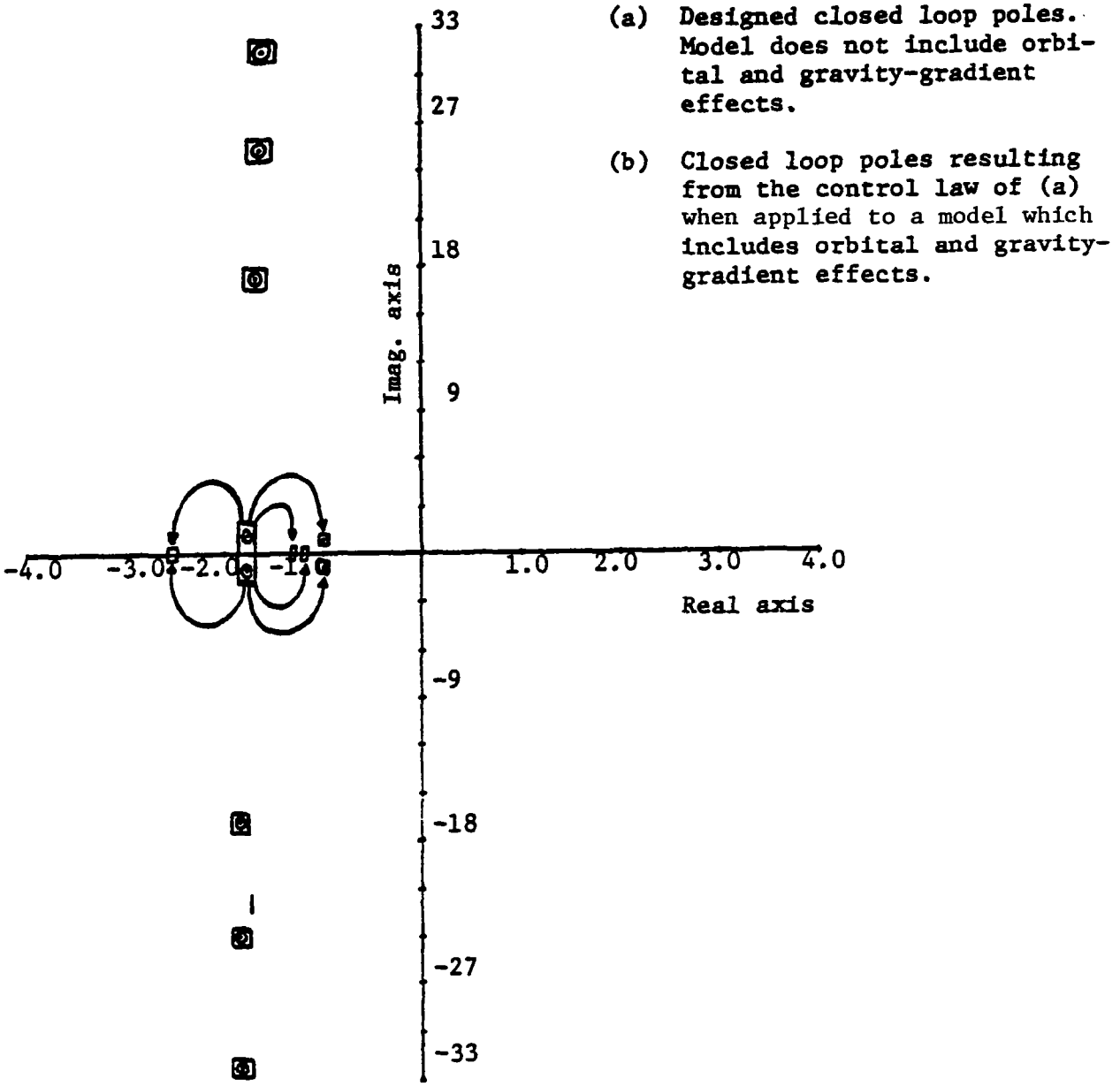

Figure 6.- Shift in closed loop poles due to orbital and gravity-gradient torques. Square plate in 250-n.-mi. orbit. Overall designed response time constant of the system = 460 sec.

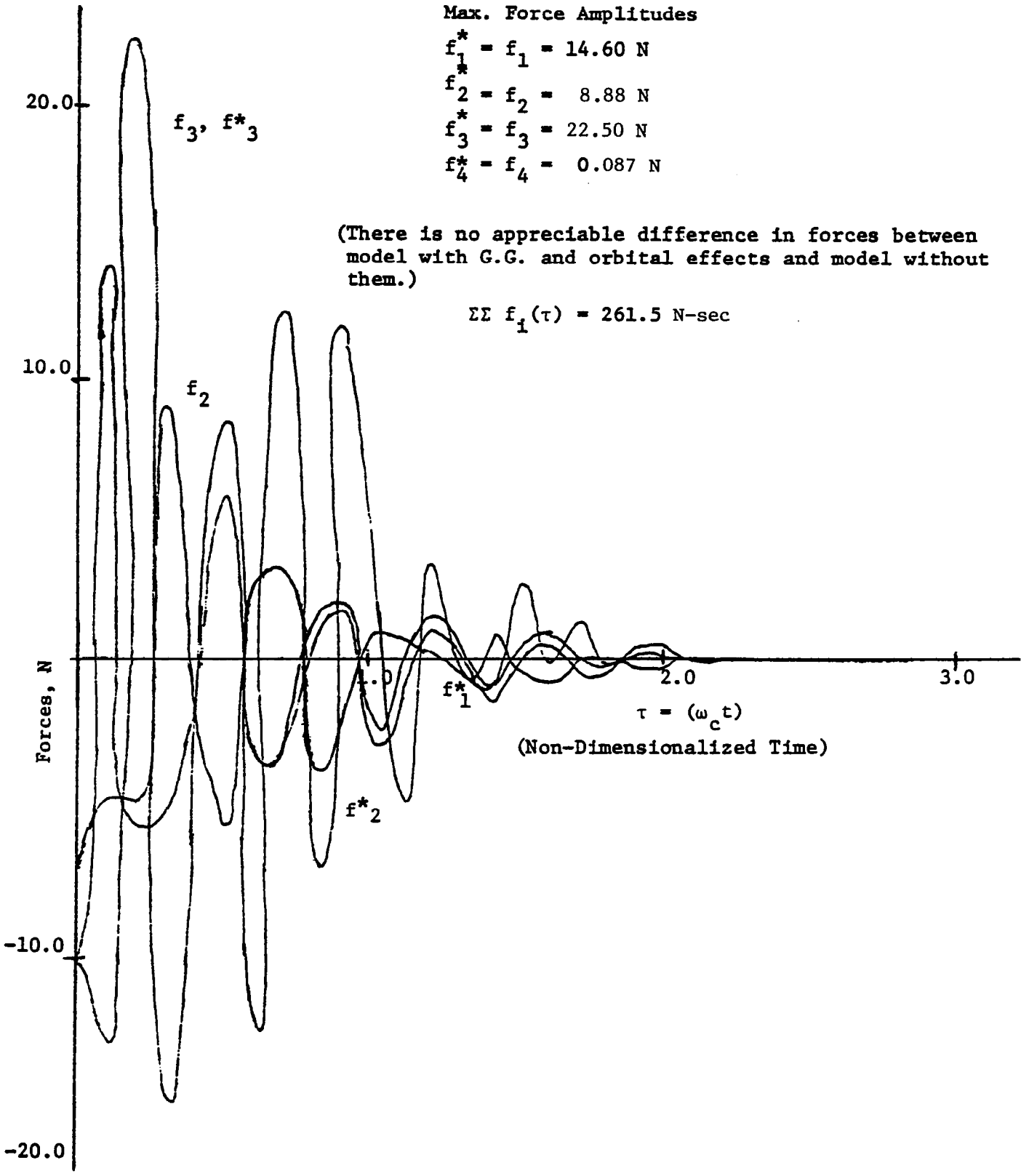

Figure 7.- Time history of control forces. Square plate.

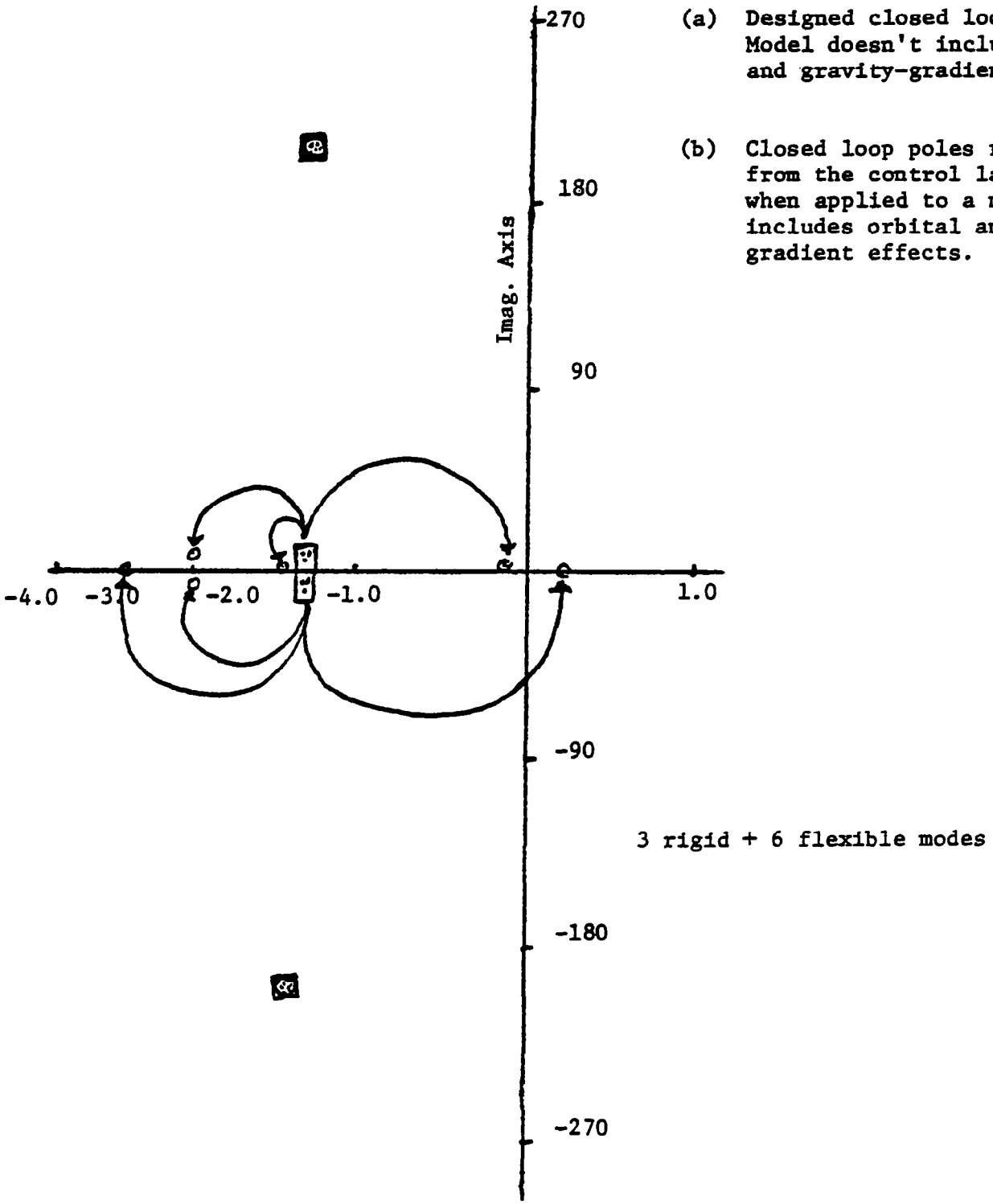

Figure 8.- Shift in closed loop poles due to orbital and gravity-gradient torques. Shallow spherical shell in 250-n.-mi. orbit. Overall designed response time constant of the system = 615.0 sec.

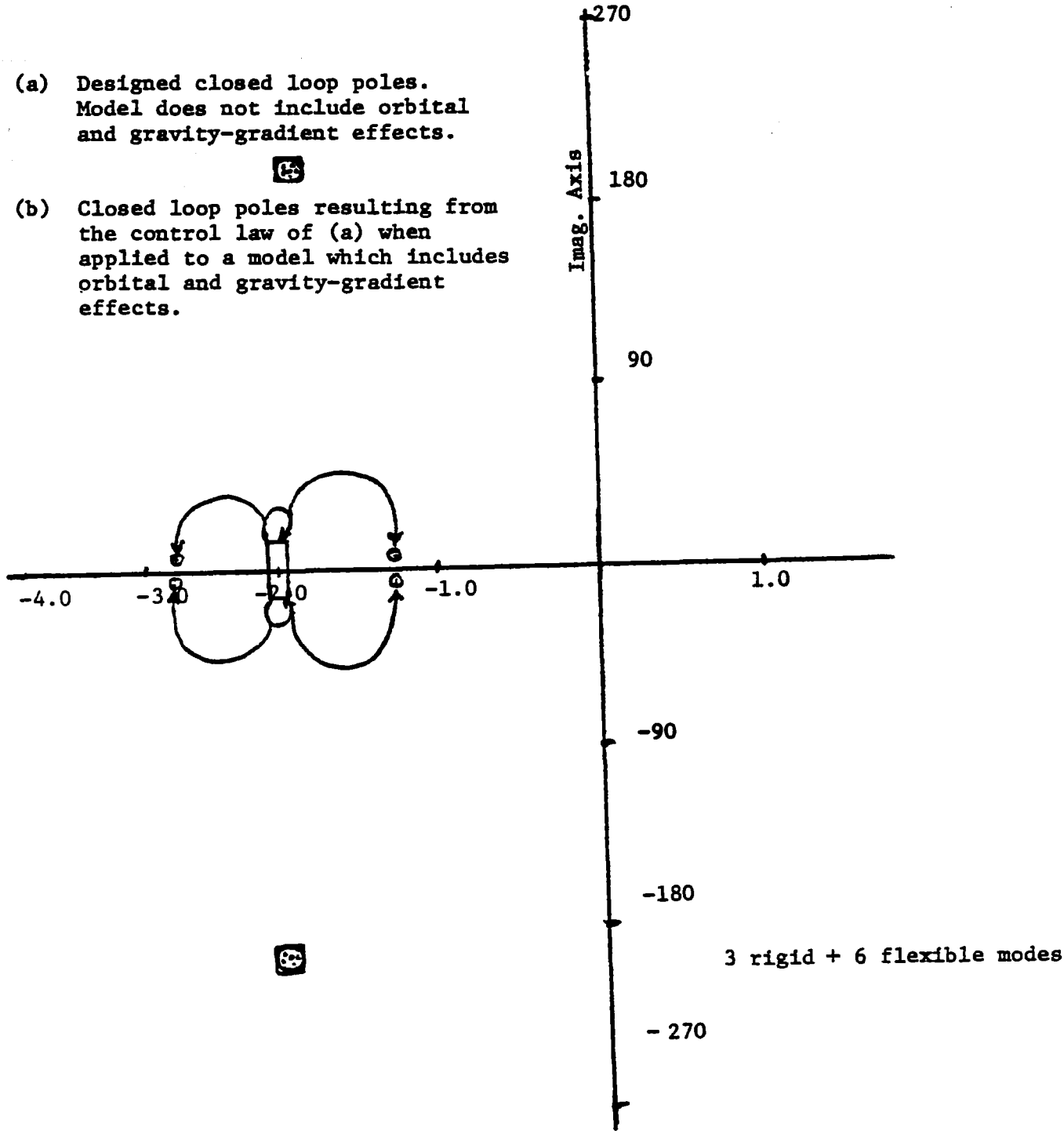

Figure 9.- Shift in closed loop poles due to orbital and gravity-gradient torques. Shallow spherical shell in 250-n.-mi. orbit. Overall designed response time constant of the system = 400 sec.

PEAK FORCE AMPLITUDES-CONTROL LAW DEVELOPED WITHOUT ORBITAL AND GRAVITY-GRADIENT EFFECTS IN THE MODEL AND THEN APPLIED TO A MODEL WITH THEM (Shell in orbit).

Without Orbital and G.G. Effects	With Orbital and G.G. Effects*
f_1: 516.40 N	f_1^*: 565.63 N
f_2: 73.30 N	f_2^*: 164.76 N
f_3: 239.50 N	f_3^*: 321.11 N
f_4: 117.54 N	f_4^*: 117.07 N
f_5: 132.45 N	f_5^*: 153.84 N
f_6: 146.82 N	f_6^*: 431.61 N
$\sum\sum_{ti} f_i$ = 7020.8 N-sec	$\sum\sum_{ti} f_i^*$ = 19373.0 N-sec

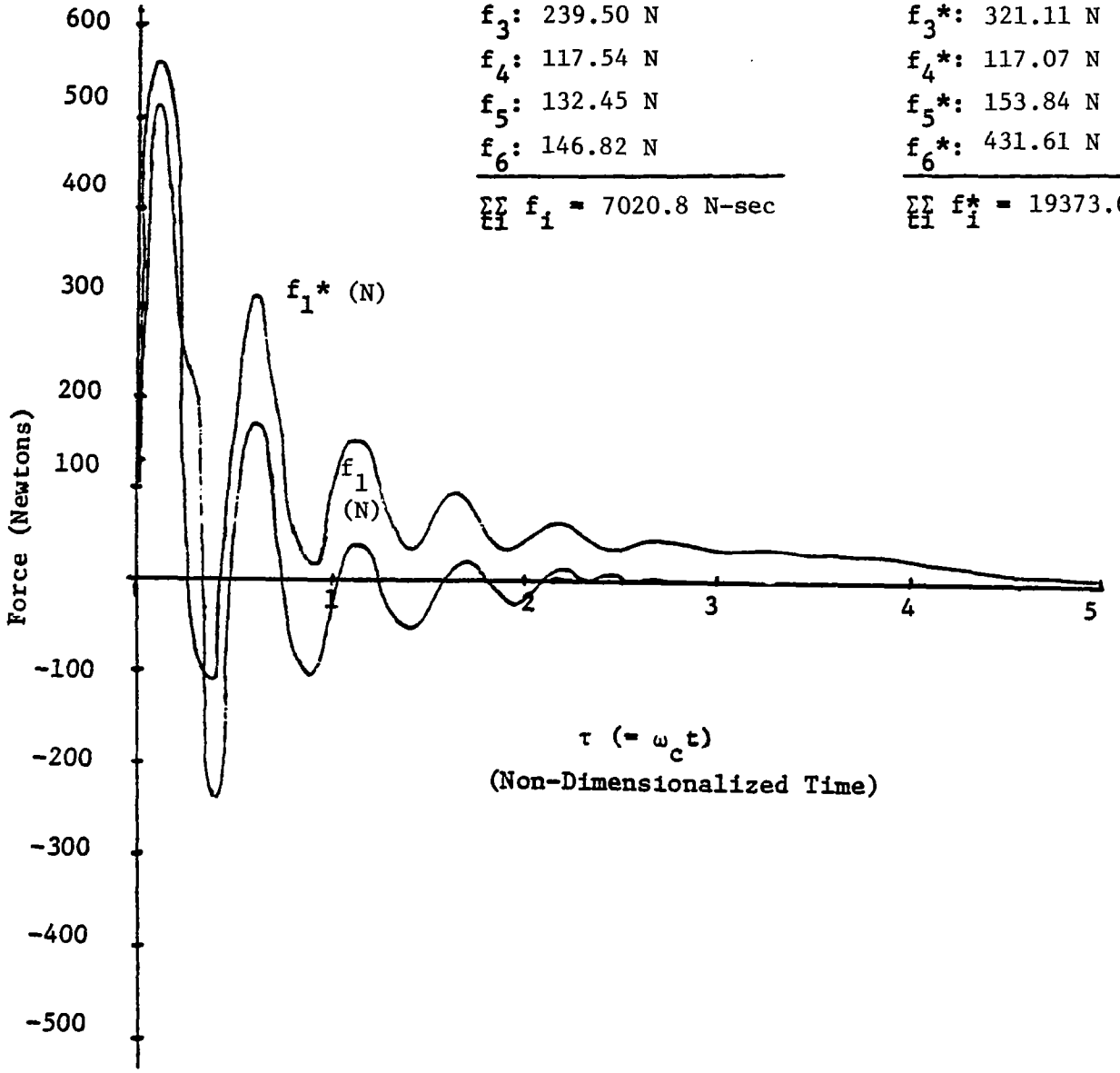

Figure 10.- Time history of control forces. Shallow spherical shell.